
Engineering Optimization
Publication details, including instructions for authors and subscription information:
http://www.tandfonline.com/loi/geno20

# The continuous adjoint approach to the k-ω SST turbulence model with applications in shape optimization

I.S. Kavvadias[a], E.M. Papoutsis-Kiachagias[a], G. Dimitrakopoulos[a] & K.C. Giannakoglou[a]

[a] Parallel CFD & Optimization Unit, Laboratory of Thermal Turbomachines, School of Mechanical Engineering, National Technical University of Athens, Greece

Published online: 08 Dec 2014.

*Engineering Optimization*, 2014
http://dx.doi.org/10.1080/0305215X.2014.979816

Taylor & Francis
Taylor & Francis Group

# The continuous adjoint approach to the *k–ω SST* turbulence model with applications in shape optimization

I.S. Kavvadias, E.M. Papoutsis-Kiachagias, G. Dimitrakopoulos and K.C. Giannakoglou*

*Parallel CFD & Optimization Unit, Laboratory of Thermal Turbomachines, School of Mechanical Engineering, National Technical University of Athens, Greece*

(*Received 29 July 2014; accepted 24 September 2014*)

In this article, the gradient of aerodynamic objective functions with respect to design variables, in problems governed by the incompressible Navier–Stokes equations coupled with the *k–ω SST* turbulence model, is computed using the continuous adjoint method, for the first time. Shape optimization problems for minimizing drag, in external aerodynamics (flows around isolated airfoils), or viscous losses in internal aerodynamics (duct flows) are considered. Sensitivity derivatives computed with the proposed adjoint method are compared to those computed with finite differences or a continuous adjoint variant based on the frequently used assumption of frozen turbulence; the latter proves the need for differentiating the turbulence model. Geometries produced by optimization runs performed with sensitivities computed by the proposed method and the 'frozen turbulence' assumption are also compared to quantify the gain from formulating and solving the adjoint to the turbulence model equations.

**Keywords:** continuous adjoint; adjoint turbulence models; sensitivity derivatives; aerodynamic shape optimization



## 1. Introduction

The computation of exact sensitivity derivatives with respect to (w.r.t.) a set of design variables, for use in optimization problems, while keeping the computational cost as low as possible is of great importance. The adjoint method is the most efficient way to compute exact sensitivities, at a cost comparable to that of the numerical solution of the state equations, irrespective of the number of design variables.

In aerodynamic optimization problems, where the state equations are the Navier–Stokes equations, both continuous formulations, where the state partial differential equations—PDEs—are firstly differentiated and then discretized (Pironneau 1984; Jameson 1988; Anderson and Venkatakrishnan 1997; Papadimitriou and Giannakoglou 2007), and discrete formulations, where the state PDEs are firstly discretized and then differentiated (Giles and Pierce 1997; Gauger *et al.* 2008; Towara and Naumann 2013), are used.

In turbulent flows, where the state PDEs comprise the Reynolds-averaged Navier–Stokes (RANS) equations coupled with a turbulence model, the turbulence model must be considered during the derivation of the adjoint equations, otherwise wrong sensitivities might be computed. In the discrete adjoint for turbulent flows, it is almost a common practice to differentiate

*Corresponding author. Email: kgianna@central.ntua.gr

the turbulence model in order to compute exact sensitivity derivatives (Anderson and Bonhaus 1999; Nielsen, Lu, and Darmofal 2004; Lee and Kim 2007; Hartmann, Held, and Leicht 2011; Naumann 2012). In contrast, when applying the continuous adjoint method to the RANS equations for turbulent flows, the differentiation of the turbulence model is often omitted (Anderson and Venkatakrishnan 1997; Jameson, Pierce, and Martinelli 1998; Papadimitriou and Giannakoglou 2007; Othmer 2008). Such an approach is referred to as the 'frozen turbulence' assumption. There is only a very limited number of recent articles on the continuous adjoint method that compute exact sensitivities by overcoming the 'frozen turbulence' assumption. For low-Reynolds number turbulence models, *i.e.* those integrating the RANS and turbulence model PDEs to the wall, the continuous adjoint to the Spalart–Allmaras turbulence model was initially presented in Zymaris *et al.* (2009) for incompressible flows and, later on, in Bueno-Orovio *et al.* (2012) for compressible flows. Also, in Kiachagias *et al.* (2014), the continuous adjoint to the Launder–Sharma $k$–$\epsilon$ turbulence model for incompressible flows was proposed. For turbulence models based on the wall functions technique, the only model differentiated with the continuous adjoint method is the $k$–$\epsilon$ turbulence model, presented in Zymaris *et al.* (2010). In the latter, in order to differentiate the wall functions, new adjoint quantities such as the adjoint friction velocity and the adjoint wall functions were introduced. In Taylor *et al.* (2013), a hybrid approach was presented in which the mean-flow equations are differentiated with the continuous adjoint method, while the turbulence model uses the discrete adjoint method.

In the present work, the steady-state $k$–$\omega$ *SST* turbulence model for incompressible flows (Menter 1994) with wall functions (Vieser, Esch, and Menter 2002; Menter, Kuntz, and Langtry 2003) is differentiated using the continuous adjoint method for the first time in the relevant literature. The same turbulence model has been differentiated in the past (Nemili *et al.* 2013) though by using the discrete adjoint method. Difficulties encountered using the continuous adjoint method are absolutely different from those using the discrete approach, and this will become clear as the article develops.

Though there are previous publications originating from the same research group on adjoints to the $k$–$\epsilon$ model (Zymaris *et al.* 2010; Papoutsis-Kiachagias *et al.* 2014) differentiating the $k$–$\omega$ *SST* model proved to be a challenge on its own. It is known that the latter combines the advantages of both the $k$–$\epsilon$ and $k$–$\omega$ models by blending them into a single one, using appropriate blending functions. These blending functions define where each model is to be used. Most difficulties in differentiating the $k$–$\omega$ *SST* model stem from the fact that these blending functions are heavily dependent on non-differentiable functions (such as *min* and *max*). Another novelty in this article is the way the wall functions model is differentiated; as seen in Section 2, this is done differently from in the $k$–$\epsilon$ model.

To switch to unsteady flows, the proposed method needs additionally to cope with the backward-in-time integration of the adjoint PDEs and the relevant storage requirements (for instance, via the check-pointing technique—see Griewank and Walther 2000). Apart from the time integration issues, the findings of this article are applicable to the unsteady flow model as well.

The proposed method is validated by conducting numerical tests in shape optimization problems. In all these tests, the accuracy of the computed objective function gradient is demonstrated, in contrast to the lack of accuracy in computations following the 'frozen turbulence' assumption. Sensitivity derivatives computed using finite differences are used as reference values.

The formulation of the adjoint method is carried out using a general objective function, so that the adaptation of the proposed method to objective functions other than those presented here is, more or less, straightforward.

## 2. State equations

The state equations are the RANS equations for the steady flow of an incompressible fluid, coupled with the *k–ω SST* model with wall functions (Menter 1994), which bridge the gap between the first cell-centre next to the wall and the corresponding wall face. The Reynolds-averaged mean flow equations are

$$R^p = -\frac{\partial v_j}{\partial x_j} = 0 \tag{1}$$

$$R_i^v = v_j \frac{\partial v_i}{\partial x_j} - \frac{\partial \tau_{ij}}{\partial x_j} + \frac{\partial p}{\partial x_i} = 0, \quad i = 1, 2(, 3), \tag{2}$$

where $v_i$ are the velocity components, $p$ the pressure divided by the constant density,

$$\tau_{ij} = (\nu + \nu_t)\left(\frac{\partial v_i}{\partial x_j} + \frac{\partial v_j}{\partial x_i}\right)$$

is the viscous stress tensor, $\nu$ the kinematic viscosity and $\nu_t$ the turbulent viscosity. Throughout this article, the Einstein convention is used, where repeated indices imply summation, unless otherwise noted.

In the *k–ω SST* model, two turbulence model PDEs complete the system of state PDEs; these are

$$R^k = v_j \frac{\partial k}{\partial x_j} - \frac{\partial}{\partial x_j}\left([\nu + \sigma_k \nu_t]\frac{\partial k}{\partial x_j}\right) - A + \beta^* \omega k = 0 \tag{3}$$

$$R^\omega = v_j \frac{\partial \omega}{\partial x_j} - \frac{\partial}{\partial x_j}\left([\nu + \sigma_\omega \nu_t]\frac{\partial \omega}{\partial x_j}\right) - \gamma \frac{\partial v_i}{\partial x_j}\left(\frac{\partial v_i}{\partial x_j} + \frac{\partial v_j}{\partial x_i}\right) + \beta\omega^2 - 2(1 - F_1)\frac{\sigma_{\omega_2}}{\omega}\frac{\partial k}{\partial x_j}\frac{\partial \omega}{\partial x_j} = 0, \tag{4}$$

where $k$ is the turbulence kinetic energy and $\omega$ is the specific dissipation rate. In the $k$ equation, $A$ depends on the generation of $k$ as follows:

$$A = \min\left(G, c_1 \beta^* \omega k\right), \tag{5}$$

where

$$G = \nu_t \frac{\partial v_i}{\partial x_j}\left(\frac{\partial v_i}{\partial x_j} + \frac{\partial v_j}{\partial x_i}\right).$$

The blending function $F_1$ is responsible for the transition from the $k$–$\omega$ model, applied near the wall, to the $k$–$\epsilon$ model applied elsewhere; it is

$$F_1 = \tanh\left(\arg_{F1}{}^4\right), \tag{6}$$

where

$$\arg_{F1} = \min\left\{\min\left[\max\left(\frac{\sqrt{k}}{\beta^* \omega d}, \frac{500\nu}{d^2 \omega}\right), \frac{4\sigma_{\omega_2} k}{d^2 \max\left(\frac{2\sigma_{\omega_2}}{\omega}\frac{\partial k}{\partial x_j}\frac{\partial \omega}{\partial x_j}, 10^{-10}\right)}\right], 10\right\}. \tag{7}$$

The turbulence viscosity coefficient $\nu_t$ is defined as

$$\nu_t = \frac{a_1 k}{\max(a_1\omega, \mathcal{S}_t F_2)}, \tag{8}$$

where

$$\mathcal{S}_t = \sqrt{\left(\frac{\partial v_i}{\partial x_j} + \frac{\partial v_j}{\partial x_i}\right)^2}$$

is the strain rate. $F_2$ is a second blending function defined, similarly to Equation (6), as

$$F_2 = \tanh(\arg_{F2}{}^2), \tag{9}$$

where

$$\arg_{F_2} = \min\left[\max\left(\frac{2\sqrt{k}}{\beta^*\omega d}, \frac{500\nu}{d^2\omega}\right), 100\right] \tag{10}$$

and $\sigma_k$, $\sigma_\omega$, $\beta$, $\beta^*$ and $\gamma$ are the model 'constants'. For each model 'constant' $\phi$, its local value is given by

$$\phi = F_1\phi_1 + (1 - F_1)\phi_2, \tag{11}$$

where $\phi_1$ and $\phi_2$ are the corresponding constants of the original $k$–$\omega$ and $k$–$\epsilon$ models, respectively.

The $k$–$\omega$ model constants are $\sigma_{k1} = 0.85034$, $\sigma_{\omega 1} = 0.5$, $\beta_1 = 0.075$, $\beta_1^* = 0.09$, $\gamma_1 = 0.5532$ and the $k$–$\epsilon$ constants are $\sigma_{k2} = 1.0$, $\sigma_{\omega 2} = 0.85616$, $\beta_2 = 0.0828$, $\beta_2^* = 0.09$, $\gamma_2 = 0.4403$. Also, $\kappa = 0.41$, $a_1 = 0.31$, $c_1 = 10.0$ (Menter 1994).

For the mean-flow equations, the SIMPLE pressure-correction algorithm (Patankar and Spalding (1972)) is employed using a cell-centred, collocated finite-volume scheme. Within each iteration, the solution of the turbulence model PDEs is decoupled from that of the mean flow equations.

To bridge the gap between the wall and the first cell centre next to the wall (point P), the wall functions technique, in the form of the 'automatic near-wall treatment' (AWT) scheme, as proposed by Vieser, Esch and Menter (2002), is used. The AWT scheme is adapted to the cell-centred finite-volume discretization scheme. According to the AWT, the value of $\omega$ at P, Figure 1, is computed as

$$\omega^P = \sqrt{\left(\frac{6\nu}{\beta_1 d^{\mathrm{P}2}}\right)^2 + \left(\frac{\sqrt{k^P}}{\beta^{*0.25}\kappa d^{\mathrm{P}}}\right)^2} \tag{12}$$

in terms of the local $k^{\mathrm{P}}$ value and the distance $d^{\mathrm{P}}$ of P from the wall.

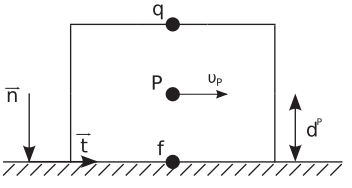


Figure 1. Finite volume adjacent to the solid wall: P is the centre of the first cell off the wall, $f$ is the boundary wall face, $\vec{n}$ is the outward unit vector normal to the wall, $\vec{t}$ is the unit tangential vector to the wall and $d^{\mathrm{P}}$ the distance between $f$ and P.

Along the wall, zero Neumann conditions for both $k$ and $\omega$ and a no-slip condition for the velocity are imposed. The velocity derivative normal to the wall is computed using a local finite-difference scheme and is then multiplied (in practice corrected) by an appropriate $\nu_t$ value at P, ensuring the computation of consistent stresses at the wall.

## 3. Objective function and its differentiation

In this article, two objective functions are used. The first is the force exerted on a solid body, projected onto the $r_i$ direction, where $r_i$ are the components of an appropriate user-defined unit vector. This objective function is defined as

$$J_F = \int_{S_W} \left( p\delta_i^j - \tau_{ij} \right) r_j n_i \, \mathrm{d}S, \tag{13}$$

where $S_W$ is the part of the wall surface where the objective function is defined, $n_j$ are the components of the unit vector which is normal to the wall pointing towards the solid and $\delta_i^j$ is the Kronecker symbol. In external aerodynamics, if $r_i$ is aligned with the farfield flow velocity, Equation (13) represents the drag force. $J_F$ may also represent lift by appropriately defining $r_i$.

The second objective function is the mass(volume)-averaged total pressure losses

$$J_{p_t} = -\int_{S_{I,O}} \left( p + \frac{1}{2} v_j^2 \right) v_i n_i \, \mathrm{d}S, \tag{14}$$

where $S_I$, $S_O$ are the inlet and outlet boundaries of the computational domain $\Omega$ and $S_{I,O} = S_I \cup S_O$.

In general, any objective function defined along $S$ can be expressed as

$$J = \int_S J_{S_i} n_i \mathrm{d}S, \tag{15}$$

where $S = S_I \cup S_O \cup S_W$. The integrand $J_{S_i} n_i$ depends on $\mathbf{n}$, which in turn may depend on shape parameterization. Differentiating $J$ w.r.t. the design variables $b_m$, $m \in [1, N]$, gives

$$\frac{\delta J}{\delta b_m} = \int_S \frac{\delta J_{S_i}}{\delta b_m} n_i \mathrm{d}S + \int_S J_{S_i} \frac{\delta n_i}{\delta b_m} \, \mathrm{d}S + \int_S J_{S_i} n_i \frac{\delta(\mathrm{d}S)}{\delta b_m}. \tag{16}$$

Along $S$, $\delta J_{S_i}/\delta b_m$ can be developed further using the relation

$$\frac{\delta \Phi}{\delta b_m} = \frac{\partial \Phi}{\partial b_m} + \frac{\partial \Phi}{\partial x_k} n_k \frac{\delta x_l}{\delta b_m} n_l, \tag{17}$$

where $\Phi$ may stand for any flow variable or the residuals of the flow equations.

Along $S_I$ and $S_O$, which are not deformed,

$$\frac{\delta x_l}{\delta b_m} = \frac{\delta n_l}{\delta b_m} = \frac{\delta \, (\mathrm{d})}{\delta b_m} = 0.$$

By taking into consideration Equation (17), after applying the chain rule for the partial derivative of $J_{S_i}$, Equation (16) takes the form

$$\begin{aligned} \frac{\delta J}{\delta b_m} = & \int_S \frac{\partial J_{S_i}}{\partial v_k} n_i \frac{\partial v_k}{\partial b_m} \, \mathrm{d}S + \int_S \frac{\partial J_{S_i}}{\partial p} n_i \frac{\partial p}{\partial b_m} \, \mathrm{d}S + \int_S \frac{\partial J_{S_i}}{\partial k} n_i \frac{\partial k}{\partial b_m} \, \mathrm{d}S + \int_S \frac{\partial J_{S_i}}{\partial \omega} n_i \frac{\partial \omega}{\partial b_m} \, \mathrm{d}S \\ & + \int_S \frac{\partial J_{S_i}}{\partial \tau_{kj}} n_i \frac{\partial \tau_{kj}}{\partial b_m} \, \mathrm{d}S + \int_{S_W} n_i \frac{\partial J_{S_{W,i}}}{\partial x_k} n_k \frac{\delta x_l}{\delta b_m} n_l \, \mathrm{d}S + \int_{S_W} J_{S_i} \frac{\delta n_i}{\delta b_m} \, \mathrm{d}S + \int_{S_W} J_{S_i} n_i \frac{\delta(\mathrm{d}S)}{\delta b_m}. \end{aligned} \tag{18}$$

## 4. The continuous adjoint method

### 4.1. *Formulation*

The starting point of the development is the augmented objective function $L$,

$$L = J + \int_{\Omega} \left( u_i R_i^v + q R^p + k_a R^k + \omega_a R^{\omega} \right) \mathrm{d}\Omega, \tag{19}$$

where $u_i$, $q$, $k_a$ and $\omega_a$ are the variables adjoint to $v_i$, $p$, $k$ and $\omega$, respectively, and $R$ are the residuals of the state equations as defined in Section 2. Since the residuals of the state equations are zero, differentiating either $L$ or $J$ w.r.t. $b_m$ is identical. Terms with the adjoint turbulence variables are not neglected, since such an assumption ('frozen turbulence') may damage the accuracy of the computed sensitivities, as shown in Section 6.

By employing the Leibniz rule for differentiation under the integral sign, the derivatives of $L$ w.r.t. $b_m$ become

$$\begin{aligned} \frac{\delta L}{\delta b_m} = \frac{\delta J}{\delta b_m} &+ \int_{\Omega} u_i \frac{\partial R_i^v}{\partial b_m} \mathrm{d}\Omega + \int_{\Omega} q \frac{\partial R^p}{\partial b_m} \mathrm{d}\Omega + \int_{\Omega} k_a \frac{\partial R^k}{\partial b_m} \mathrm{d}\Omega + \int_{\Omega} \omega_a \frac{\partial R^{\omega}}{\partial b_m} \mathrm{d}\Omega \\ &+ \int_{S} \left( u_i R_i^v + q R^p + k_a R^k + \omega_a R^{\omega} \right) \frac{\delta x_k}{\delta b_m} n_k \, \mathrm{d}S. \end{aligned} \tag{20}$$

By substituting the derivatives of the primal equations' residuals w.r.t. $b_m$ into Equation (20), and after the necessary rearrangements which are omitted herein, the following is obtained:

$$\begin{aligned} \frac{\delta L}{\delta b_m} = \frac{\delta J}{\delta b_m} &+ \int_{\Omega} u_i \frac{\partial v_i}{\partial x_j} \frac{\partial v_j}{\partial b_m} \mathrm{d}\Omega + \int_{\Omega} u_i v_j \frac{\partial}{\partial x_j} \left( \frac{\partial v_i}{\partial b_m} \right) \mathrm{d}\Omega \\ &+ \int_{\Omega} u_i \frac{\partial}{\partial x_i} \left( \frac{\partial p}{\partial b_m} \right) \mathrm{d}\Omega - \int_{\Omega} u_i \frac{\partial}{\partial x_j} \left[ \left( \frac{\partial v_i}{\partial x_j} + \frac{\partial v_j}{\partial x_i} \right) \frac{\partial \nu_t}{\partial b_m} \right] \mathrm{d}\Omega \\ &- \int_{\Omega} u_i \frac{\partial}{\partial x_j} \left( (\nu + \nu_t) \left[ \frac{\partial}{\partial x_j} \left( \frac{\partial v_i}{\partial b_m} \right) \right] \right) \mathrm{d}\Omega \\ &- \int_{\Omega} u_i \frac{\partial}{\partial x_j} \left( (\nu + \nu_t) \left[ \frac{\partial}{\partial x_i} \left( \frac{\partial v_j}{\partial b_m} \right) \right] \right) \mathrm{d}\Omega - \int_{\Omega} q \frac{\partial}{\partial x_j} \left( \frac{\partial v_j}{\partial b_m} \right) \mathrm{d}\Omega \\ &+ \int_{\Omega} k_a \frac{\partial k}{\partial x_j} \frac{\partial v_j}{\partial b_m} \mathrm{d}\Omega + \int_{\Omega} k_a v_j \frac{\partial}{\partial x_j} \left( \frac{\partial k}{\partial b_m} \right) \mathrm{d}\Omega - \int_{\Omega} k_a \frac{\partial A}{\partial b_m} \mathrm{d}\Omega \\ &+ \int_{\Omega} \beta^* k_a k \frac{\partial \omega}{\partial b_m} \mathrm{d}\Omega + \int_{\Omega} \beta^* k_a \omega \frac{\partial k}{\partial b_m} \mathrm{d}\Omega \\ &- \int_{\Omega} k_a \frac{\partial}{\partial x_j} \left( \nu_t \frac{\partial k}{\partial x_j} \frac{\partial \sigma_k}{\partial b_m} \right) \mathrm{d}\Omega - \int_{\Omega} k_a \frac{\partial}{\partial x_j} \left( \sigma_k \frac{\partial k}{\partial x_j} \frac{\partial \nu_t}{\partial b_m} \right) \mathrm{d}\Omega \\ &- \int_{\Omega} k_a \frac{\partial}{\partial x_j} \left( [\nu + \sigma_k \nu_t] \frac{\partial}{\partial x_j} \left( \frac{\partial k}{\partial b_m} \right) \right) \mathrm{d}\Omega + \int_{\Omega} \omega_a \frac{\partial \omega}{\partial x_j} \frac{\partial v_j}{\partial b_m} \mathrm{d}\Omega \\ &+ \int_{\Omega} \omega_a v_j \frac{\partial}{\partial x_j} \left( \frac{\partial \omega}{\partial b_m} \right) \mathrm{d}\Omega - \int_{\Omega} \omega_a \frac{\partial v_i}{\partial x_j} \left( \frac{\partial v_i}{\partial x_j} + \frac{\partial v_j}{\partial x_i} \right) \frac{\partial \gamma}{\partial b_m} \mathrm{d}\Omega \\ &- \int_{\Omega} 2\gamma \omega_a \left( \frac{\partial v_i}{\partial x_j} + \frac{\partial v_j}{\partial x_i} \right) \frac{\partial}{\partial x_j} \left( \frac{\partial v_i}{\partial b_m} \right) \mathrm{d}\Omega + \int_{\Omega} \omega_a \omega^2 \frac{\partial \beta}{\partial b_m} \mathrm{d}\Omega \end{aligned}$$

$$
\begin{aligned}
&+\int_\Omega 2\beta\omega_a\omega\frac{\partial\omega}{\partial b_m}\,\mathrm{d}\Omega-\int_\Omega\omega_a\frac{\partial}{\partial x_j}\left(\nu_t\frac{\partial\omega}{\partial x_j}\frac{\partial\sigma_\omega}{\partial b_m}\right)\mathrm{d}\Omega\\
&-\int_\Omega\omega_a\frac{\partial}{\partial x_j}\left(\sigma_\omega\frac{\partial\omega}{\partial x_j}\frac{\partial\nu_t}{\partial b_m}\right)\mathrm{d}\Omega-\int_\Omega\omega_a\frac{\partial}{\partial x_j}\left([\nu+\sigma_\omega\nu_t]\frac{\partial}{\partial x_j}\left(\frac{\partial\omega}{\partial b_m}\right)\right)\mathrm{d}\Omega\\
&+\int_\Omega 2\omega_a\frac{\sigma_{\omega_2}}{\omega}\frac{\partial k}{\partial x_j}\frac{\partial\omega}{\partial x_j}\frac{\partial F_1}{\partial b_m}\,\mathrm{d}\Omega+\int_\Omega 2\omega_a(1-F_1)\frac{\sigma_{\omega_2}}{\omega}\frac{\partial k}{\partial x_j}\frac{\partial\omega}{\partial x_j}\frac{\partial\omega}{\partial b_m}\,\mathrm{d}\Omega\\
&-\int_\Omega 2\omega_a(1-F_1)\frac{\sigma_{\omega_2}}{\omega}\frac{\partial\omega}{\partial x_j}\frac{\partial}{\partial x_j}\left(\frac{\partial k}{\partial b_m}\right)\mathrm{d}\Omega\\
&-\int_\Omega 2\omega_a(1-F_1)\frac{\sigma_{\omega_2}}{\omega}\frac{\partial k}{\partial x_j}\frac{\partial}{\partial x_j}\left(\frac{\partial\omega}{\partial b_m}\right)\mathrm{d}\Omega+\int_S T_k^1\frac{\delta x_k}{\delta b_m}\,\mathrm{d}S,
\end{aligned}
\tag{21}
$$

where $T_k^1=(u_iR_i^\nu+qR^p+k_aR^k+\omega_aR^\omega)n_k$.

A distinguishing feature of the *k–ω SST* model, which is a major difficulty in developing the adjoint equations, is that it includes quantities, such as those defined in Equations (5), (7), (8) and (10), which are not differentiable. For instance, the derivative of $A$, Equation (5), w.r.t. $b_m$, is

$$
\frac{\partial A}{\partial b_m}=\frac{\partial\nu_i}{\partial x_j}\left(\frac{\partial\nu_i}{\partial x_j}+\frac{\partial\nu_j}{\partial x_i}\right)\frac{\partial\nu_t}{\partial b_m}+2\nu_t\left(\frac{\partial\nu_i}{\partial x_j}+\frac{\partial\nu_j}{\partial x_i}\right)\frac{\partial}{\partial x_j}\left(\frac{\partial\nu_i}{\partial b_m}\right)
\tag{22}
$$

if $G<c_1\beta^*\omega k$, or

$$
\frac{\partial A}{\partial b_m}=c_1\beta^*k\frac{\partial\omega}{\partial b_m}+c_1\beta^*\omega\frac{\partial k}{\partial b_m}
\tag{23}
$$

otherwise.

Regarding the turbulent viscosity coefficient, $\nu_t=\nu_t(k,\omega,\mathcal{S}_t)$, this is generally written as

$$
\frac{\partial\nu_t}{\partial b_m}=\frac{\partial\nu_t}{\partial k}\frac{\partial k}{\partial b_m}+\frac{\partial\nu_t}{\partial\omega}\frac{\partial\omega}{\partial b_m}+\frac{\partial\nu_t}{\partial\mathcal{S}_t}\frac{\partial\mathcal{S}_t}{\partial b_m}.
\tag{24}
$$

Any further development of Equation (24) must account for the different expressions the denominator of Equation (8) may take on.

The $F_1$ blending function is differentiated in the same way, namely

$$
\frac{\partial F_1}{\partial b_m}=\frac{\partial F_1}{\partial k}\frac{\partial k}{\partial b_m}+\frac{\partial F_1}{\partial\omega}\frac{\partial\omega}{\partial b_m}.
\tag{25}
$$

For the 'constants' $\phi$ of the *k–ω SST* model, embodying the blending expressed by Equation (11) yields

$$
\frac{\partial\phi}{\partial F_1}=\phi_1-\phi_2=\phi^\Delta.
$$

By substituting Equations (22) to (25) into Equation (21), applying the Green–Gauss theorem where necessary, reordering, grouping the terms accordingly and considering also Equation (18),

the following is obtained:

$$\begin{aligned}\frac{\delta L}{\delta b_m} &= \int_\Omega \left( R_i^u \frac{\partial v_i}{\partial b_m} + R^q \frac{\partial p}{\partial b_m} + R^{k_a} \frac{\partial k}{\partial b_m} + R^{\omega_a} \frac{\partial \omega}{\partial b_m} \right) \mathrm{d}\Omega \\ &+ \int_S D_i^u \frac{\partial v_i}{\partial b_m} \mathrm{d}S + \int_S D^q \frac{\partial p}{\partial b_m} \mathrm{d}S + \int_S D^{k_a} \frac{\partial k}{\partial b_m} \mathrm{d}S + \int_S D^{\omega_a} \frac{\partial \omega}{\partial b_m} \mathrm{d}S \\ &+ \int_S \left( \frac{\partial J_{S_k}}{\partial \tau_{ij}} n_k - u_i n_j \right) \frac{\partial \tau_{ij}}{\partial b_m} \mathrm{d}S - \int_S k_a \left[ \nu + \sigma_k \nu_t \right] \frac{\partial}{\partial b_m} \left( \frac{\partial k}{\partial x_j} \right) n_j \mathrm{d}S \\ &- \int_S \omega_a \left[ \nu + \sigma_\omega \nu_t \right] \frac{\partial}{\partial b_m} \left( \frac{\partial \omega}{\partial x_j} \right) n_j \mathrm{d}S + \int_{S_W} T_k^1 \frac{\delta x_k}{\delta b_m} \mathrm{d}S \\ &+ \int_{S_W} n_i \frac{\partial J_{S_{W,i}}}{\partial x_k} n_k \frac{\delta x_l}{\delta b_m} n_l \mathrm{d}S + \int_{S_W} J_{S_i} \frac{\delta n_i}{\delta b_m} \mathrm{d}S + \int_{S_W} J_{S_i} n_i \frac{\delta (\mathrm{d}S)}{\delta b_m}. \end{aligned} \tag{26}$$

Eliminating the coefficients of

$$\frac{\partial v_i}{\partial b_m}, \frac{\partial p}{\partial b_m}, \frac{\partial k}{\partial b_m} \quad \text{and} \quad \frac{\partial \omega}{\partial b_m}$$

from the field integrals results in the field adjoint equations (see Section 4.2). All coefficients, based on which the adjoint boundary conditions are derived, are denoted by $D$ with various superscripts. In the interest of saving space, their lengthy expressions are omitted since the interested reader can derive them by her/himself.

### 4.2. *Field adjoint equations*

By eliminating all variations in the mean flow and turbulence model variables from the field integrals of Equation (26), the field adjoint equations are derived. These are listed below:

$$R^q = -\frac{\partial u_j}{\partial x_j} = 0 \tag{27a}$$

$$\begin{aligned} R_i^u &= -v_j \frac{\partial u_i}{\partial x_j} + u_j \frac{\partial v_i}{\partial x_j} - \frac{\partial \tau_{ij}^a}{\partial x_j} + \frac{\partial q}{\partial x_i} + k_a \frac{\partial k}{\partial x_j} + \omega_a \frac{\partial \omega}{\partial x_j} \\ &+ 2 \frac{\partial}{\partial x_j} \left[ \left( M_1 k_a \nu_t + \gamma \omega_a + M_3 \frac{C_{\Omega,\nu_t} a_1 k}{2 \mathcal{S}_t^3 F_2} \right) \left( \frac{\partial v_i}{\partial x_j} + \frac{\partial v_j}{\partial x_i} \right) \right] = 0 \end{aligned} \tag{27b}$$

$$\begin{aligned} R^{k_a} &= -v_j \frac{\partial k_a}{\partial x_j} - \frac{\partial}{\partial x_j} \left( \left[ \nu + \sigma_k \nu_t \right] \frac{\partial k_a}{\partial x_j} \right) + 2 \frac{\partial}{\partial x_j} \left( \omega_a \left[ 1 - F_1 \right] \frac{\sigma_{\omega_2}}{\omega} \frac{\partial \omega}{\partial x_j} \right) \\ &+ (1 - M_2 c_1) \beta^* k_a \omega + \frac{\partial \nu_t}{\partial k} C_{\Omega,\nu_t} + \frac{\partial F_1}{\partial k} C_{\Omega,F_1} = 0 \end{aligned} \tag{27c}$$

$$\begin{aligned} R^{\omega_a} &= -v_j \frac{\partial \omega_a}{\partial x_j} - \frac{\partial}{\partial x_j} \left( \left[ \nu + \sigma_\omega \nu_t \right] \frac{\partial \omega_a}{\partial x_j} \right) + 2 \frac{\partial}{\partial x_j} \left( \omega_a \left[ 1 - F_1 \right] \frac{\sigma_{\omega_2}}{\omega} \frac{\partial k}{\partial x_j} \right) \\ &+ 2 \omega_a (1 - F_1) \frac{\sigma_{\omega_2}}{\omega^2} \frac{\partial k}{\partial x_j} \frac{\partial \omega}{\partial x_j} + 2 \beta \omega_a \omega + (1 - M_2 c_1) \beta^* k_a k \\ &+ \frac{\partial \nu_t}{\partial \omega} C_{\Omega,\nu_t} + \frac{\partial F_1}{\partial \omega} C_{\Omega,F_1} = 0. \end{aligned} \tag{27d}$$

In the above equations,

$$\tau_{ij}^{a} = (\nu + \nu_t)\left(\frac{\partial u_i}{\partial x_j} + \frac{\partial u_j}{\partial x_i}\right)$$

is the adjoint viscous stress tensor and a number of extra terms (denoted by $M_l, l = 1, 2, 3$, $C_{\Omega,\nu_t}$ and $C_{\Omega,F_1}$) appear. These are defined as follows:

$$C_{\Omega,\nu_t} = \frac{\partial u_i}{\partial x_j}\left(\frac{\partial \nu_i}{\partial x_j} + \frac{\partial \nu_j}{\partial x_i}\right) + \sigma_k \frac{\partial k}{\partial x_j}\frac{\partial k_a}{\partial x_j} + \sigma_\omega \frac{\partial \omega}{\partial x_j}\frac{\partial \omega_a}{\partial x_j} - M_1 k_a \frac{\partial \nu_i}{\partial x_j}\left(\frac{\partial \nu_i}{\partial x_j} + \frac{\partial \nu_j}{\partial x_i}\right) \tag{28a}$$

$$C_{\Omega,F_1} = \nu_t \sigma_k^{\Delta} \frac{\partial k_a}{\partial x_j}\frac{\partial k}{\partial x_j} - \gamma^{\Delta}\omega_a \frac{\partial \nu_i}{\partial x_j}\left(\frac{\partial \nu_i}{\partial x_j} + \frac{\partial \nu_j}{\partial x_i}\right) + \beta^{\Delta}\omega_a\omega^2 + \nu_t \sigma_\omega^{\Delta}\frac{\partial \omega_a}{\partial x_j}\frac{\partial \omega}{\partial x_j} + 2\omega_a \frac{\sigma_{\omega_2}}{\omega}\frac{\partial k}{\partial x_j}\frac{\partial \omega}{\partial x_j}. \tag{28b}$$

Also,

$$M_1 = 1 - M_2 = \begin{cases} 1, & \text{if } G < c_1\beta^*\omega k \\ 0, & \text{else} \end{cases} \quad \text{and} \quad M_3 = \begin{cases} 1, & \text{if } \mathcal{S}_t F_2 > a_1\omega \\ 0, & \text{else.} \end{cases}$$

Closed form expressions for $\partial\nu_t/\partial k$, $\partial F_1/\partial k$, $\partial\nu_t/\partial\omega$ and $\partial F_1/\partial\omega$ can be derived.

### 4.3. *Adjoint boundary conditions*

By eliminating the coefficients of the variations in the mean flow and turbulence model variables from the various boundary integrals of Equation (26), the adjoint boundary conditions are derived.

#### 4.3.1. *Inlet conditions*

Along the inlet boundary $S_I$, due to the Dirichlet conditions on $\nu_i$, $k$ and $\omega$, the $S_I$ parts of the first, third and fourth boundary integrals of Equation (26) are automatically eliminated. The third and sixth integrals are eliminated by satisfying the following set of conditions:

$$u_j n_j = -\frac{\partial J_{S_{I,i}}}{\partial p} n_i \tag{29a}$$

$$u_i t_i^{\mathrm{I}} = \frac{\partial J_{S_{I,k}}}{\partial \tau_{ij}} n_k t_i^{\mathrm{I}} n_j + \frac{\partial J_{S_{I,k}}}{\partial \tau_{ij}} n_k t_j^{\mathrm{I}} n_i \tag{29b}$$

$$u_i t_i^{\mathrm{II}} = \frac{\partial J_{S_{I,k}}}{\partial \tau_{ij}} n_k t_i^{\mathrm{II}} n_j + \frac{\partial J_{S_{I,k}}}{\partial \tau_{ij}} n_k t_j^{\mathrm{II}} n_i, \tag{29c}$$

where $t_i^{\mathrm{I}}, t_i^{\mathrm{II}}$ are the two components (in 3D cases) of the unit vectors tangent to the surface. The first tangent vector $t_i^{\mathrm{I}}$ can be defined arbitrarily whereas $t_i^{\mathrm{II}}$ results from $t_i^{\mathrm{II}} = e_{ijk} n_j t_k^{\mathrm{I}}$, $e_{ijk}$ being the permutation symbol. To eliminate the sixth and seventh boundary integrals, it suffices to impose $k_a = \omega_a = 0$.

#### 4.3.2. *Outlet conditions*

In Equation (26), the second, sixth and seventh boundary integrals along $S_O$ are eliminated due to the fixed back pressure and the zero Neumann conditions for $k$ and $\omega$. By assuming a uniform velocity profile at $S_O$, the fifth boundary integral in Equation (26) may vanish too.

To eliminate the remaining integrals along $S_O$, which depend on $\partial v_i/\partial b_m$, $\partial k/\partial b_m$ and $\partial \omega/\partial b_m$, the following conditions are imposed:

$$u_i v_j n_j + (\nu+\nu_t)\left(\frac{\partial v_i}{\partial x_j}+\frac{\partial v_j}{\partial x_i}\right)n_j - q n_i + \frac{\partial J_{S_{O,k}}}{\partial v_i}n_k - 2\left(M_1 \nu_t k_a + \gamma \omega_a + M_3 \frac{C_{\Omega,\nu_t} a_1 k}{2S^3 F_2}\right)\left(\frac{\partial v_i}{\partial x_j}+\frac{\partial v_j}{\partial x_i}\right)n_j = 0 \tag{30a}$$

$$v_j n_j k_a + [\nu + \sigma_k \nu_t]\frac{\partial k_a}{\partial x_j}n_j + \frac{\partial J_{S_{O,j}}}{\partial k}n_j = 0 \tag{30b}$$

$$v_j n_j \omega_a + [\nu + \sigma_\omega \nu_t]\frac{\partial \omega_a}{\partial x_j}n_j + \frac{\partial J_{S_{O,j}}}{\partial \omega}n_j = 0. \tag{30c}$$

### 4.3.3. *Wall conditions*

The derivation of the $k_a$ and $\omega_a$ boundary conditions starts from Equation (12), which specifies $\omega$ at the cell-centre P (Figure 1). Recall also that, at the boundary face of the finite-volume centred at P, zero Neumann conditions are imposed on both $k$ and $\omega$.

As in the primal solver, it is assumed here that all state equations are integrated up to the wall; so the second, third, fourth and fifth surface integrals written along $S_W$ are eliminated by satisfying the following equations:

$$u_j n_j = -\frac{\partial J_{S_{W,i}}}{\partial p}n_i \tag{31a}$$

$$u_i t_i^{\mathrm{I}} = \frac{\partial J_{S_{W,k}}}{\partial \tau_{ij}}n_k t_i^{\mathrm{I}} n_j + \frac{\partial J_{S_{W,k}}}{\partial \tau_{ij}}n_k t_j^{\mathrm{I}} n_i \tag{31b}$$

$$u_i t_i^{\mathrm{II}} = \frac{\partial J_{S_{W,k}}}{\partial \tau_{ij}}n_k t_i^{\mathrm{II}} n_j + \frac{\partial J_{S_{W,k}}}{\partial \tau_{ij}}n_k t_j^{\mathrm{II}} n_i \tag{31c}$$

$$[\nu + \sigma_k \nu_t]\frac{\partial k_a}{\partial x_j}n_j = -\frac{\partial J_{S_{W,j}}}{\partial k}n_j \tag{31d}$$

$$[\nu + \sigma_\omega \nu_t]\frac{\partial \omega_a}{\partial x_j}n_j = -\frac{\partial J_{S_{W,j}}}{\partial \omega}n_j. \tag{31e}$$

In case the objective function does not depend directly on turbulence quantities, the last two conditions degenerate to zero Neumann conditions for $k_a$ and $\omega_a$. Next, the differentiation of the AWT is taken into consideration which, for the first row of cells off the solid walls (centre P in Figure 1), leads to the condition

$$\omega_a + \frac{\partial \nu_t}{\partial \omega}C_{\Omega,\nu_t} + \frac{\partial F_1}{\partial \omega}C_{\Omega,F_1} = 0. \tag{32}$$

This condition for $\omega_a$ at P must be understood as the 'adjoint AWT'. It is interesting to notice that, as in the state PDEs where a specific expression is used to compute $\omega$ at P, the duality of the adjoint equations produces a specific expression for $\omega_a$ for P, Equation (32).

### 4.4. *Sensitivity derivatives*

After eliminating all other integrals, by satisfying the field adjoint equations and the adjoint boundary conditions, the final expression for the sensitivity derivatives becomes

$$\begin{aligned}
\frac{\delta J}{\delta b_m} = &- \int_{S_W} \left( \tau_{ij}^a n_j - q n_i - M_3 \frac{C_{\Omega,\nu_t} a_1 k}{S^3 F_2} \left( \frac{\partial v_i}{\partial x_j} + \frac{\partial v_j}{\partial x_i} \right) n_j \right) \frac{\partial v_i}{\partial x_k} n_k \frac{\delta x_l}{\delta b_m} n_l \, \mathrm{d}S + T_w \\
&+ \int_{S_W} k_a \left[ \nu + \sigma_k \nu_t \right] \frac{\partial}{\partial x_k} \left( \frac{\partial k}{\partial x_j} n_j \right) \frac{\delta x_k}{\delta b_m} \, \mathrm{d}S + \int_{S_W} k_a \left[ \nu + \sigma_k \nu_t \right] \frac{\partial k}{\partial x_j} \frac{\delta n_j}{\delta b_m} \, \mathrm{d}S \\
&+ \int_{S_W} \omega_a \left[ \nu + \sigma_\omega \nu_t \right] \frac{\partial}{\partial x_k} \left( \frac{\partial \omega}{\partial x_j} n_j \right) \frac{\delta x_k}{\delta b_m} \, \mathrm{d}S + \int_{S_W} \omega_a \left[ \nu + \sigma_\omega \nu_t \right] \frac{\partial \omega}{\partial x_j} \frac{\delta n_j}{\delta b_m} \, \mathrm{d}S \\
&+ \int_{S_W} n_i \frac{\partial J_{S_i}}{\partial x_k} n_k \frac{\delta x_l}{\delta b_m} n_l \, \mathrm{d}S + \int_{S_W} J_{S_i} \frac{\delta n_i}{\delta b_m} \, \mathrm{d}S + \int_{S_W} J_{S_i} n_i \frac{\delta (\mathrm{d}S)}{\delta b_m} + \int_{S_W} T_k^1 \frac{\delta x_k}{\delta b_m} \, \mathrm{d}S \\
&- \int_{S_W} \left[ \left( -u_k n_k + \frac{\partial J_{S_k}}{\partial \tau_{lz}} n_k n_l n_z \right) \left( \tau_{ij} \frac{\delta (n_i n_j)}{\delta b_m} + \frac{\partial \tau_{ij}}{\partial x_z} n_z \frac{\delta x_k}{\delta b_m} n_k n_i n_j \right) \right] \mathrm{d}S \\
&- \int_{S_W} \left[ \frac{\partial J_{S_k}}{\partial \tau_{lz}} n_k t_l^{\mathrm{I}} t_z^{\mathrm{I}} \left( \tau_{ij} \frac{\delta (t_i^{\mathrm{I}} t_j^{\mathrm{I}})}{\delta b_m} + \frac{\partial \tau_{ij}}{\partial x_z} n_z \frac{\delta x_k}{\delta b_m} n_k t_i^{\mathrm{I}} t_j^{\mathrm{I}} \right) \right] \mathrm{d}S \\
&- \int_{S_W} \left[ \left( \frac{\partial J_{S_k}}{\partial \tau_{lz}} n_k (t_l^{\mathrm{II}} t_z^{\mathrm{I}} + t_l^{\mathrm{I}} t_z^{\mathrm{II}}) \right) \left( \tau_{ij} \frac{\delta (t_i^{\mathrm{II}} t_j^{\mathrm{I}})}{\delta b_m} + \frac{\partial \tau_{ij}}{\partial x_z} n_z \frac{\delta x_k}{\delta b_m} n_k t_i^{\mathrm{II}} t_j^{\mathrm{I}} \right) \right] \mathrm{d}S \\
&- \int_{S_W} \left[ \frac{\partial J_{S_k}}{\partial \tau_{lz}} n_k t_l^{\mathrm{II}} t_z^{\mathrm{II}} \left( \tau_{ij} \frac{\delta (t_i^{\mathrm{II}} t_j^{\mathrm{II}})}{\delta b_m} + \frac{\partial \tau_{ij}}{\partial x_z} n_z \frac{\delta x_k}{\delta b_m} n_k t_i^{\mathrm{II}} t_j^{\mathrm{II}} \right) \right] \mathrm{d}S, \qquad (33)
\end{aligned}$$

where $T_w$ includes terms originating from the differentiation of the wall functions technique. The first integral on the right-hand side of Equation (33) results for the condition

$$\frac{\partial v_i}{\partial b_m} = -\frac{\partial v_i}{\partial x_k} n_k \frac{\delta x_l}{\delta b_m} n_l$$

(Equation 17) along $S_W$. The last four $S_W$ integrals emerge during the derivation of Equations (31b) and (31c).

In shape optimization, if the design variables are the coordinates of the Bézier–Bernstein control points, then $\delta x_k / \delta b_m$ can be computed analytically by differentiating the parameterization equation(s). Then, to compute sensitivity derivatives w.r.t. the normal displacement of the boundary wall nodes in discrete form,

$$\frac{\delta x_{kq}}{\delta b_m} = \frac{\delta x_{kq}}{\delta x_{lm}} n_{lm} = n_{qk},$$

where $q, m \in [1, N]$ and $k, l = 1, 2(, 3)$ (no summation over $m$).

## 5. Optimization algorithm

The sensitivity derivatives computed with the proposed adjoint method have been incorporated into the following optimization algorithm.

(1) The state equations, Equations (1) and (2), are numerically solved.
(2) The objective function $J$, Equation (15), is computed.
(3) The adjoint equations, Equations (27a)–(27d), are numerically solved.
(4) The sensitivity derivatives $\delta J/\delta b_m$ are computed, Equation (33).
(5) The design variables, $b_m$, are updated.
(6) The computational grid is updated.
(7) Go to step 1.

For the update of the design variables in each optimization cycle, the steepest descent scheme is used. Other faster variants, such as the conjugate gradient method (Nocedal and Wright 1999) or limited memory quasi-Newton methods (Steward *et al.* 2012) could be used instead. However, any study on the convergence rate of descent algorithms is beyond the scope of this article; the main concern is how accurately to compute sensitivity derivatives by also differentiating the *k–ω SST* model.

For the update of the computational grid within each optimization cycle, the Laplace equation for nodal displacement is solved. The boundary conditions for the Laplace equation are the known displacements of the parameterized wall nodes together with zero displacements at any other boundary node.

Some of the presented applications include inequality (thickness) constraints, which are imposed using the augmented Lagrangian multipliers (ALM) method with penalty functions (Nocedal and Wright 1999). An optimization problem with inequality constraints of the form

$$\min J, \text{s.t. } C_i \geq 0, i = 1, \ldots, l, \tag{34}$$

where $C_i$ is the $i$th constraint function, can be transformed into an optimization problem with equality constraints, namely

$$\min J, \text{s.t. } C_i + z_i^2 = 0, i = 1, \ldots, l, \tag{35}$$

with $z_i$ being extra variables whose optimal values must also be computed.

The optimization problem of Equations (35) can be handled as an unconstrained minimization problem aiming at the minimization of

$$L_c = J + \lambda_i \left(C_i + z_i^2\right) + w_p \left(C_i + z_i^2\right)^2, \tag{36}$$

where the $\lambda_i$ coefficients are Lagrange multipliers and $w_p$ is a penalty coefficient. The values of $\lambda_i$, $z_i^2$ and $w_p$ are updated in each optimization cycle as $\lambda_i^{k+1} = \max(\lambda_i^k - 2w_p C_i, 0)$, $z_i^2 = \max(-\lambda_i/2w_p + C_i, 0)$ and $w_p^{k+1} = \gamma w_p^k$, where $\gamma > 1$ is a user-defined value.

## 6. Applications

At first, the accuracy with which the proposed adjoint method computes the gradient of the objective function gradient is assessed.

For the drag objective function, Equation (13), the NACA0012 and the NACA4415 isolated airfoil cases are used to validate the method. The sensitivity derivatives computed with the proposed adjoint method are validated against those obtained by finite differences (reference values) and compared with the outcome of the adjoint method based on the 'frozen turbulence' assumption. The sensitivity derivatives resulting from finite differences are computed by recontouring the parameterized geometry and maintaining the same internal grid nodes in $\Omega$. For the first case, an optimization with inequality thickness constraints is performed starting from the NACA0012 airfoil.

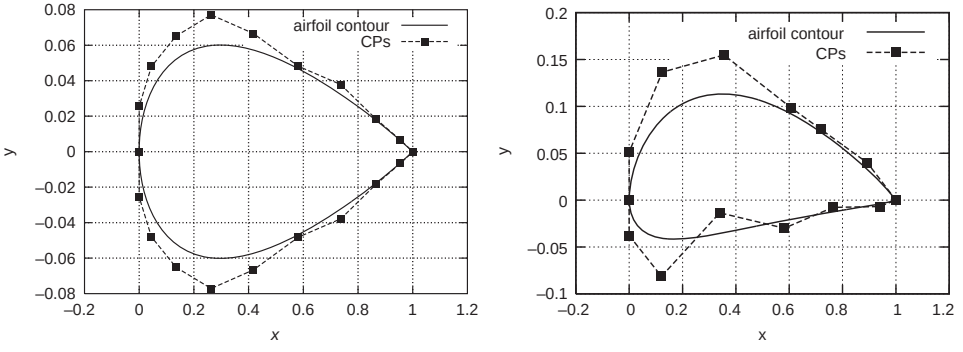


Figure 2. The NACA0012 (left) and the NACA4415 (right) airfoils, parameterized using Bézier polynomials with 12 and 8 control points, respectively, for either side (*x*- and *y*-axes not in scale). For the NACA0012 airfoil, the two last control points at the trailing edge are very close to each other, and thus indistinguishable. The sensitivity derivatives are computed w.r.t. the *x*- and *y*-coordinates of the Bézier control points, giving rise to a total of 48 (NACA0012) and 32 (NACA4415) design variables.

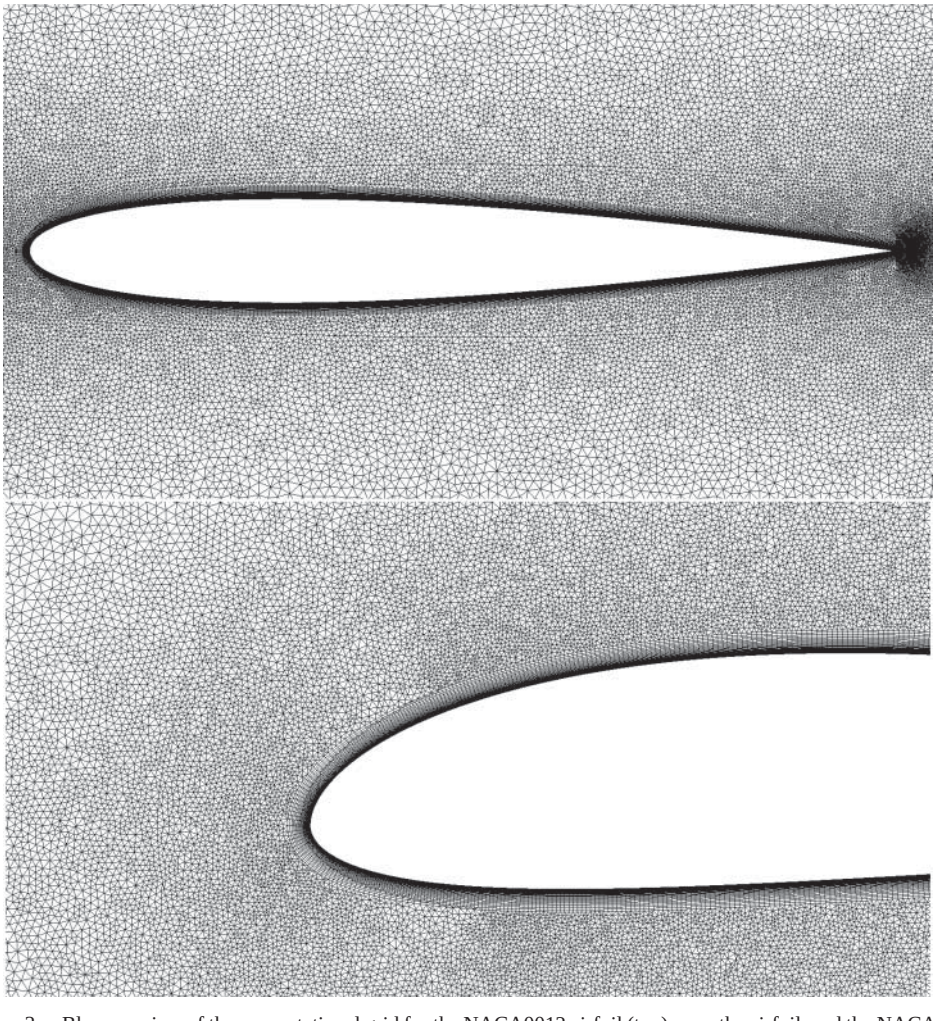

Figure 3. Blow-up view of the computational grid for the NACA0012 airfoil (top), near the airfoil, and the NACA4415 airfoil (bottom), near the leading edge.

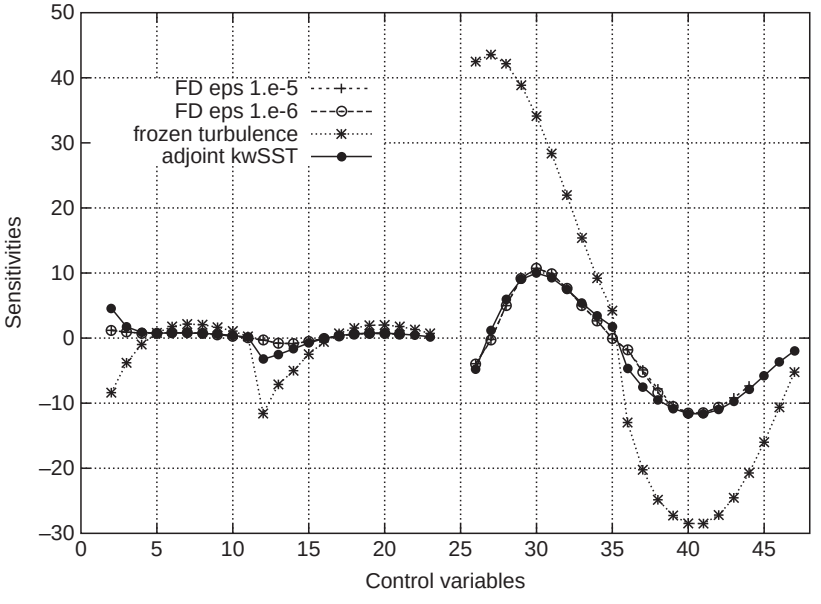


Figure 4. Drag sensitivities for the NACA0012 airfoil: the proposed method (adjoint *k–ω SST*) is compared with FD (with two step epsilon values) and the outcome of the 'frozen turbulence' adjoint.

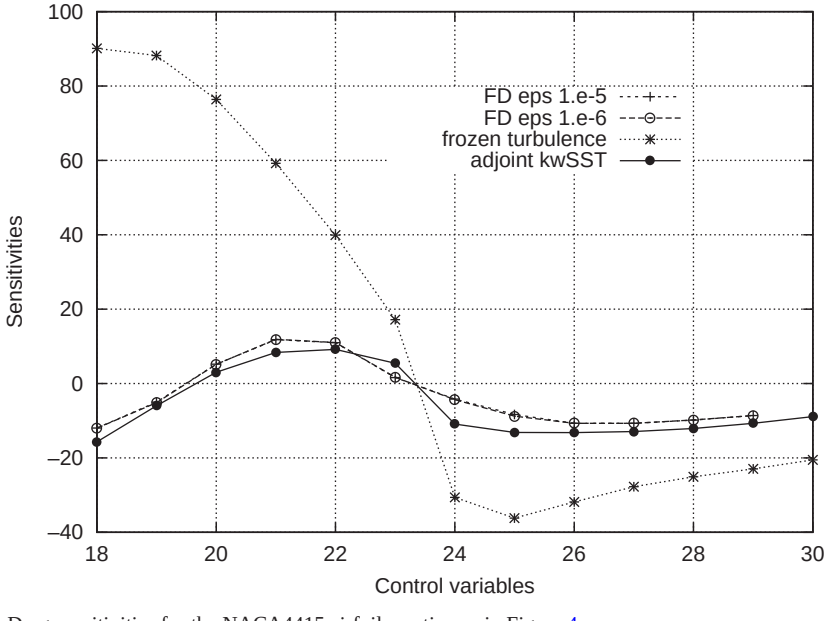


Figure 5. Drag sensitivities for the NACA4415 airfoil: caption as in Figure 4.

Both NACA0012 and NACA4415 airfoil cases have a Reynolds number $\mathrm{Re} = 6 \times 10^6$, infinite flow angle equal to $3^\circ$ and average $y^+$ of the first grid cell centres off the wall around 10.

The initial geometry of the two airfoils was approximated by best fitting Bézier polynomials. The same approximated airfoil contours were used for the validation of the proposed method. The Bézier control polygons can be seen in Figure 2. In both cases, unstructured, hybrid grids of about 200,000 cells each were used, Figure 3.

Table 1. Drag sensitivities for the NACA0012 airfoil: the FD eps 1.e−5 and FD eps 1.e−6 columns show the values of the computed sensitivity derivatives, using finite differences, as in Figure 4. Columns Adj. *k–ω SST*/FD and Frozen turb./FD show those computed by the adjoint *k–ω SST* model and the 'frozen turbulence' adjoint, respectively, divided by the corresponding FD eps 1.e−5 values. Regarding the last two columns, the ideal value is 1.

| Design variable | FD eps 1.e−5 | FD eps 1.e−6 | Adj. *k–ω SST*/FD | Frozen turb./FD |
|---|---|---|---|---|
| 4 | 0.7755 | 0.7750 | 1.154 | −1.262 |
| 7 | 0.8234 | 0.8239 | 0.9649 | 2.606 |
| 10 | 0.3112 | 0.3112 | 1.299 | 3.464 |
| 13 | −0.7921 | −0.7922 | 3.190 | 8.990 |
| 15 | −0.5138 | −0.5138 | 1.441 | 4.834 |
| 18 | 0.6079 | 0.6076 | 1.080 | 2.549 |
| 21 | 0.5781 | 0.5782 | 1.099 | 3.070 |
| 28 | 4.994 | 4.984 | 1.189 | 8.439 |
| 31 | 9.860 | 9.877 | 0.9393 | 2.876 |
| 34 | 2.634 | 2.636 | 1.289 | 3.492 |
| 37 | −4.900 | −5.213 | 1.540 | 4.128 |
| 40 | −11.53 | −11.53 | 1.004 | 2.470 |

The computed sensitivity derivatives for the initial airfoils are presented in Figures 4 and 5. The first half design variables correspond to the *x*-coordinates of the Bézier control points, from the leading to the trailing edge, first for the suction and then for the pressure side, and the rest are for the *y*-coordinates of the same control points. Finite differences were computed for epsilon (step) values of $10^{-5}$ and $10^{-6}$, denoted by 'FD eps 1.e–5' and 'FD eps 1.e–6', respectively. Since the computed sensitivity derivatives are practically the same for both of them, the finite differences are considered to be safe for use as reference derivatives. The sensitivity derivatives computed using the adjoint based on the 'frozen turbulence' assumption are way off the reference distribution, even having the wrong sign for some control points. On the other hand, the proposed method is able to reproduce the outcome of finite differences with very good accuracy. Some of the computed sensitivity derivatives for the NACA0012 airfoil are also given in Table 1.

For the NACA0012 case, an optimization run with inequality thickness constraints imposed on the objective function was then performed. According to the imposed constraints, the optimal

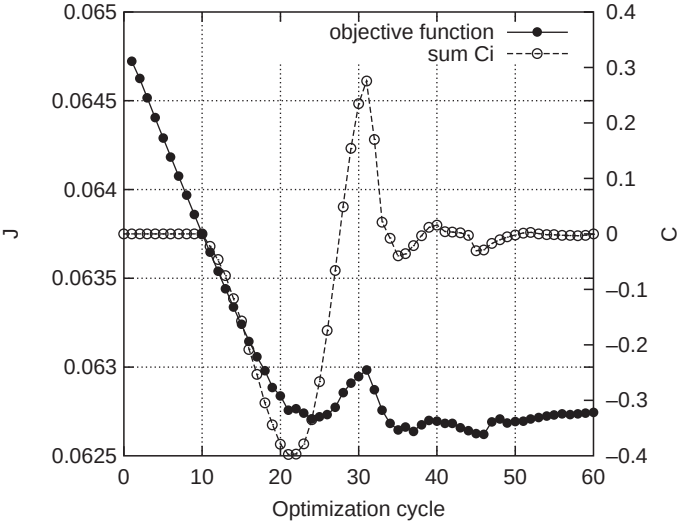


Figure 6. Objective function convergence for the NACA0012 airfoil case for the drag objective function with thickness constraints. In order to minimize the drag exerted on the airfoil, the optimization loop mainly reduces the thickness of the airfoil, up to the point where the constraints is marginally satisfied. After that, drag is reduced, while trying to satisfy the thickness constraints. At the end of the optimization, the thickness constraints are certainly satisfied.

geometry should not be thinner than a fixed percentage of the initial airfoil at some arbitrarily chosen cuts in the chordwise direction. The constraints used (as in Equation 34) are expressed as

$$C_i = T_{Ri} - T_{\mathrm{MIN}i}, \tag{37}$$

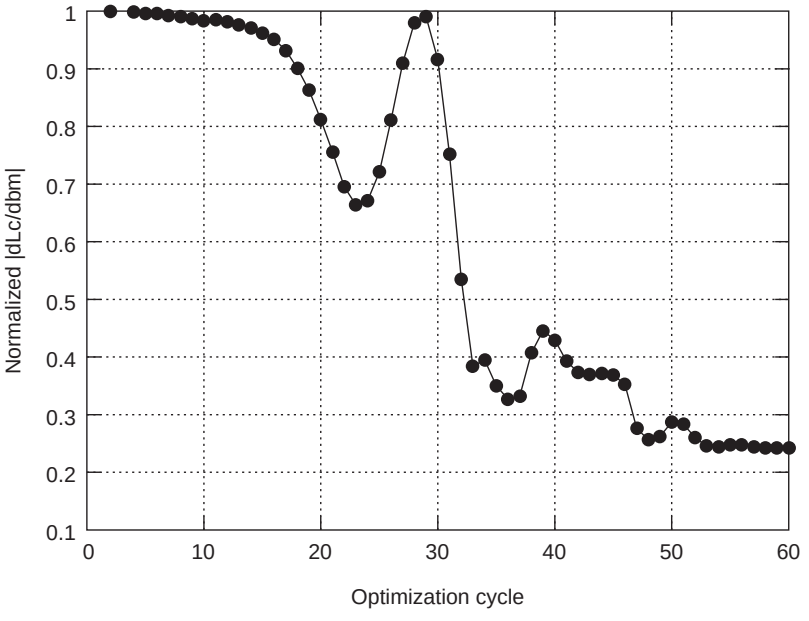


Figure 7. Normalized magnitude of the sensitivity derivatives vector for the NACA0012 airfoil case for the drag objective function with thickness constraints. Normalization was based on the sensitivity derivatives vector magnitude of the first cycle.

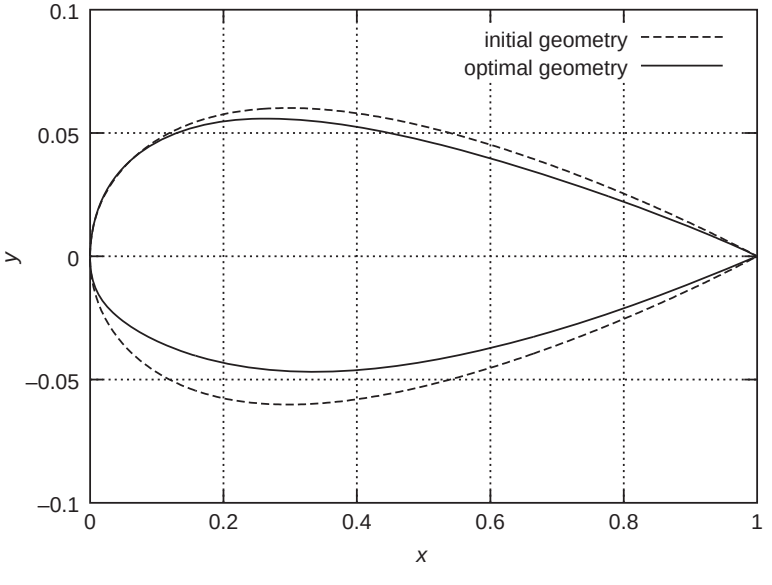


Figure 8. Contours for the initial and optimized airfoil geometries for the optimization performed on the NACA0012 airfoil. The optimal geometry is thinner than the initial geometry, as expected, while the final thickness is no less than 85% of the initial thickness, as dictated by the constraints functions.

where $T_{Ri}$ is the relative thickness and $T_{\mathrm{MIN}i}$ the minimum relative thickness allowed at cut $i$. $T_{Ri}$ is normalized by the corresponding thickness of the initial airfoil. In this application, the thickness constraints were applied at nine cuts along the chord, every 10% of the chord, from 10 up to 90%. At each cut, the target thickness was set to $T_{\mathrm{MIN}i} = 0.85$.

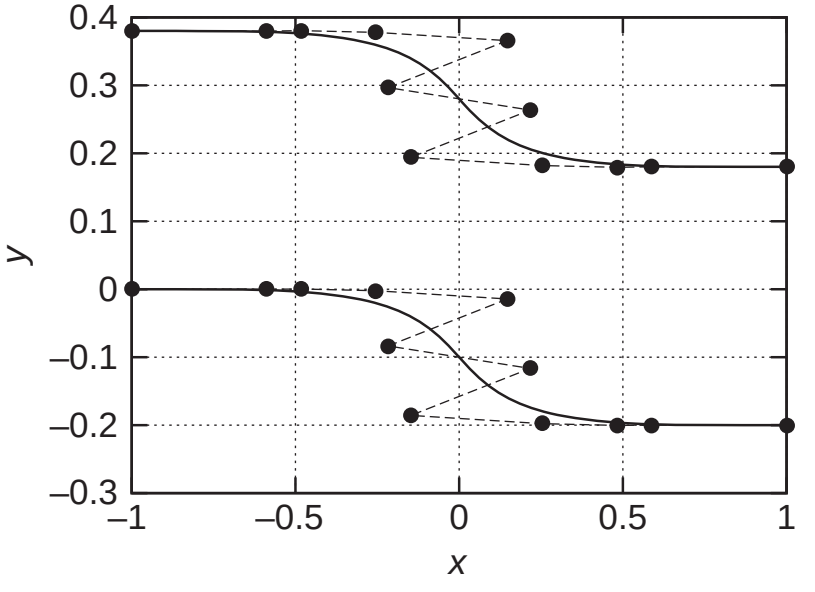


Figure 9. S-shaped duct: The duct geometry is parameterized using Bezier polynomials. 24 control points are used in total, 12 for the upper and 12 for the lower wall. Sensitivity derivatives are computed w.r.t. the $x$ and $y$ coordinates of the Bezier control points. The duct spans from about $-2$ to 2 in the $x$ direction, but only its curved part was allowed to vary during the optimization loop. Axes not in scale.

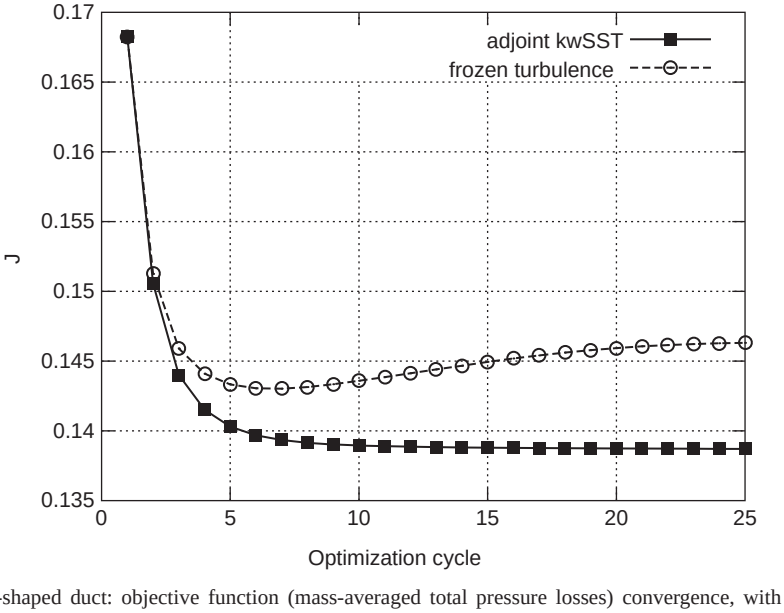


Figure 10. S-shaped duct: objective function (mass-averaged total pressure losses) convergence, with sensitivities computed with the proposed adjoint method and the 'frozen turbulence' assumption. The difference between the convergence point of the two methods are attributed to differences in accuracy between the computed sensitivities.

Since the constraints used are purely geometrical, derivatives $\delta C_i/\delta b_m$ can be analytically computed, where $b_m$ are Bézier control point coordinates.

The progress of the optimization run is shown in Figure 6 and the normalized magnitude of the sensitivity derivatives vector for each optimization iteration in Figure 7. In Figure 8, initial and optimal geometries are illustrated.

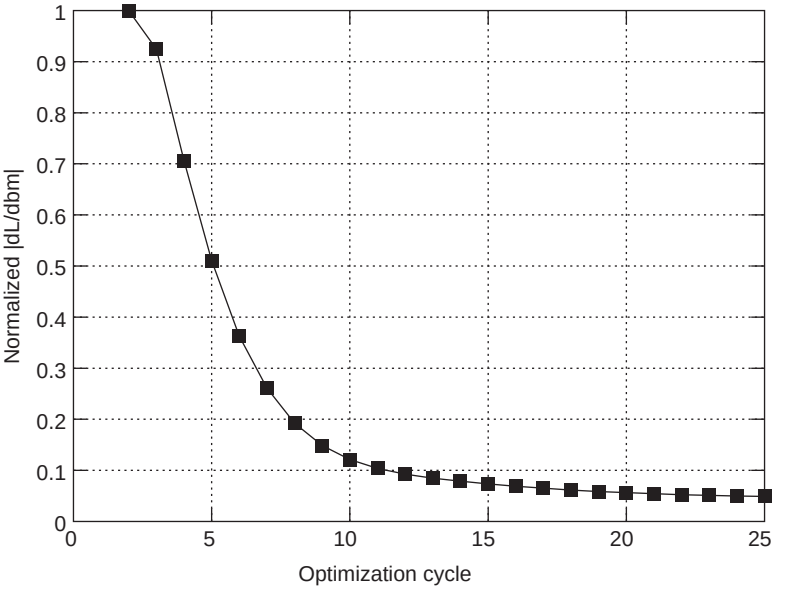


Figure 11. S-shaped duct: normalized magnitude of the sensitivity derivatives vector for mass-averaged total pressure losses. Normalization as in Figure 7.

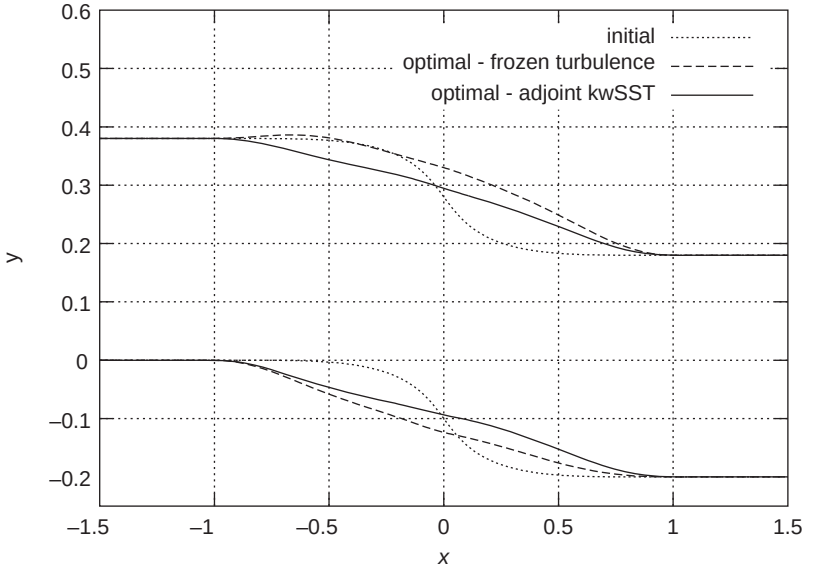


Figure 12. S-shaped duct: contours of the initial and optimal S-shaped duct geometries. In the optimal geometries, the change in the duct cross-section is milder compared to the initial one. Also, the S-turn has been smoothed out in order to minimize total pressure losses. The geometries produced by the two methods are different, which explains the difference seen in the optimal objective function values in Figure 10.

In the second part of this section, an internal aerodynamics optimization problem is tackled. This time, the total pressure losses objective function, Equation (14), was used and the optimization of a 2D S-shaped duct geometry was carried out. The S-shaped part of the duct can be seen in Figure 9, together with the Bezier control points used for the parameterization. The Reynolds number of the flow is $\mathrm{Re} = 10^5$, based on the inlet velocity and inlet width, with an average $y^+$ of the first cell centre off the wall of about 35. The evolution of the optimization run can be seen in Figure 10, the normalized magnitude of the sensitivity derivatives vector for each optimization iteration in Figure 11 and a comparison of the initial and optimal geometries in Figure 12. The 'frozen turbulence' assumption computes 'less accurate' sensitivities which lead the optimization run to a local minimum. More or less, the proposed method is able finally to locate a better solution for the same number of optimization cycles (*i.e.* for the same CPU cost; in fact, the proposed method could have been stopped somewhat earlier if a stopping criterion had been used).

## 7. Conclusions

The continuous adjoint formulation for shape optimization problems governed by the steady-state incompressible fluid flow equations and the *k–ω SST* turbulence model with wall functions was presented.

The sensitivities computed using the proposed method closely match the reference values computed by finite differences. On the other hand, the sensitivities computed using the 'frozen turbulence' assumption were less accurate and even wrongly signed in some areas, which could seriously mislead the design process, as in the S-shaped duct example.

Differentiating the *k–ω SST* turbulence model using the continuous adjoint approach was really challenging. At a first glance, this sounds almost impossible since it requires analytical differentiation of the non-differentiable *min* and *max* functions. Nevertheless, it has been proved that the continuous adjoint method can successfully be applied to this model and accurate sensitivity derivatives can be computed. Moreover, the wall functions technique was included in the derivation, which makes the proposed method a valuable tool for sensitivity analysis and optimization, even in industrial applications where the wall functions model is frequently used. In the state equations, the AWT, adapted to a cell-centred discretization scheme, leads to an expression for $\omega$, at the first cell centres off the wall, in terms of the local $k$ and distance values. The proposed formulation led to the 'adjoint AWT' condition, which is used to compute the adjoint to the $\omega$ quantity, at the same cell centres.

## References

Anderson, W. K., and D. L. Bonhaus. 1999. "Airfoil Design on Unstructured Grids for Turbulent Flows." *AIAA Journal* 37 (2): 185–191.

Anderson, W. K., and V. Venkatakrishnan. 1997. "Aerodynamic Design Optimization on Unstructured Grids with a Continuous Adjoint Formulation." In *Proceedings of the 35th AIAA Aerospace Sciences Meeting & Exhibit*, 6–9 January 1997, Reno, NV, AIAA Paper No. 97-0643. doi:10.2514/6.1997-643.

Bueno-Orovio, A., C. Castro, F. Palacios, and E. ZuaZua. 2012. "Continuous Adjoint Approach for the Spalart–Allmaras Model in Aerodynamic Optimization." *AIAA Journal* 50 (3): 631–646.

Gauger, N. R., A. Walther, C. Moldanhauer, and M. Wildhalm. 2008. "Automatic Differentiation of an Entire Design Chain for Aerodynamic Shape Optimization." *New Results in Numerical and Experimental Fluid Mechanics VI*, Contributions to the 15th STAB/DGLR Symposium, Darmstadt, Germany, 2006, Vol. 96 of Notes on Numerical Fluid Mechanics and Multidisciplinary Design (NNFM), 454–461. Berlin: Springer.

Giles, M. B., and N. A. Pierce. 1997. "Adjoint Equations in CFD: Duality, Boundary Conditions and Solution Behaviour." In *Proceedings of the 13th Computational Fluid Dynamics Conference*, Snowmass Village, CO, AIAA Paper No. 97-1850. doi:10.2514/6.1997-1850.

Griewank, A., and A. Walther. 2000. "Algorithm 799: Revolve: An Implementation of Checkpointing for the Reverse or Adjoint Mode of Computational Differentiation." *ACM Transactions on Mathematical Software (TOMS)* 26 (1): 19–45.

Hartmann, R., J. Held, and T. Leicht. 2011. "Adjoint-Based Error Estimation and Adaptive Mesh Refinement for the RANS and $k$–$\omega$ Turbulence Model Equations." *Journal of Computational Physics* 230: 4268–4284.

Jameson, A. 1988. "Aerodynamic Design via Control Theory." *Journal of Scientific Computing* 3 (3): 233–260.

Jameson, A., N. Pierce, and L. Martinelli. 1998. "Optimum Aerodynamic Design Using the Navier–Stokes Equations." *Theoretical and Computational Fluid Dynamics* 10 (1): 213–237.

Lee, B. J., and C. Kim. 2007. "Automated Design Methodology of Turbulent Internal Flow Using Discrete Adjoint Formulation." *Aerospace Science and Technology* 11 (2–3): 163–173.

Menter, F. R. 1994. "Two-Equation Eddy-Viscosity Turbulence Models for Engineering Applications." *AIAA Journal* 32 (8): 269–289.

Menter, F. R., M. Kuntz, and R. Langtry. 2003. "Ten Years of Industrial Experience with the SST Turbulence Model." *Turbulence, Heat and Mass Transfer* 4: 625–632.

Naumann, U. 2012. *U.N.: The Art of Differentiating Computer Programs*. SIAM.

Nemili, A., E. Ozkaya, N. R. Gauger, F. Kramer, A. Carnarius, and F. Thiele. 2013. "Discrete Adjoint Based Sensitivity Analysis for Optimal Flow Control of a 3D High-Lift Configuration." In *Proceedings of the 21st AIAA Computational Fluid Dynamics Conference*, San Diego, CA. AIAA Paper No. 13-2585. doi:10.2514/6.2013-2585.

Nielsen, E. J., J. Lu, M. A. Park, and D. L. Darmofal. 2004. "An Implicit Exact Dual Adjoint Solution Method for Turbulent Flows on Unstructured Grids." *Computers & Fluids* 33: 1131–1155.

Nocedal, J., and S. J. Wright. 1999. *Numerical Optimization.* New York: Springer.

Othmer, C. 2008. "A Continuous Adjoint Formulation for the Computation of Topological and Surface Sensitivities of Ducted Flows." *International Journal for Numerical Methods in Fluids* 58 (8): 861–877.

Papadimitriou, D. I., and K. C. Giannakoglou. 2007. "A Continuous Adjoint Method with Objective Function Derivatives Based on Boundary Integrals for Inviscid and Viscous Flows." *Journal of Computers & Fluids* 36 (2): 325–341.

Papoutsis-Kiachagias, E. M., A. S. Zymaris, I. S. Kavvadias, D. I. Papadimitriou, and K. C. Giannakoglou. 2014. "The Continuous Adjoint Approach to the $k$–$\epsilon$ Turbulence Model for Shape Optimization and Optimal Active Control of Turbulent Flows." *Engineering Optimization* doi:10.1080/0305215X.2014.892595.

Patankar, S. V., and D. B. Spalding. 1972. "Calculation Procedure for Heat, Mass and Momentum Transfer in Three-Dimensional Parabolic Flows." *International Journal of Heat and Mass Transfer* 15 (10): 1787–1806.

Pironneau, O. 1984. *Optimal Shape Design for Elliptic Systems.* New York: Springer-Verlag.

Steward, J. L., I. M. Navon, M. Zupanski, and N. Karmitsa. 2012. "Impact of Non-Smooth Observation Operators on Variational and Sequential Data Assimilation for a Limited-Area Shallow Water Equations Model." *Quarterly Journal of the Royal Meteorological Society* 138 (663): 323–339. doi:10.1002/qj.935.

Taylor, T. W. R., F. Palacios, K. Duraisami, and J. J. Alonso. 2013. "A Hybrid Adjoint Approach Applied to Turbulent Flow Simulations." In *Proceedings of the 21st AIAA Computational Fluid Dynamics Conference*, San Diego, CA, AIAA Paper No. 13-2452. doi:10.2514/6.2013-2452.

Towara, M., and U. Naumann. 2013. "A Discrete Adjoint Model for OpenFOAM." *Procedia Computer Science* 18 (2013): 429–438. doi:10.1016/j.procs.2013.05.206.

Vieser, W., T. Esch, and F. R. Menter. 2002. "Heat Transfer Predictions Using Advanced Two-Equation Turbulence Models." CFX Technical Memorandum CFX-VAL10/0602, AEA Technology, Otterfing, Germany.

Zymaris, A. S., D. I. Papadimitriou, K. C. Giannakoglou, and C. Othmer. 2009. "Continuous Adjoint Approach to the Spalart–Allmaras Turbulence Model for Incompressible Flows." *Computers & Fluids* 38 (8): 1528–1538.

Zymaris, A. S., D. I. Papadimitriou, K. C. Giannakoglou, and C. Othmer. 2010. "Adjoint Wall Functions: A New Concept for Use in Aerodynamic Shape Optimization." *Journal of Computational Physics* 229 (13): 5228–5245.